Inorg. Chem. **2006**, *45*, 9493–9501

Strong Electronic Communication by Direct Metal–Metal Interaction in Molecules with Halide-Bridged Dimolybdenum Pairs

F. Albert Cotton,*,† Chun Y. Liu,*,†,‡ Carlos A. Murillo,*,† and Qinliang Zhao†

Department of Chemistry, Laboratory for Molecular Structure and Bonding, P.O. Box 30012, Texas A&M University, College Station, Texas 77842-3012, and Department of Chemistry, Tongji University, Shanghai 200092, P. R. China

Received July 14, 2006

Reactions of [*cis*-$Mo_2(DAniF)_2(NCCH_3)_4](BF_4)_2$, DAniF = *N*,*N*′-di-*p*-anisylformamidinate, with an excess of anhydrous Bu^n_4NX (X = Cl, Br, I), produced the halide-bridged tetranuclear clusters, [*cis*-$Mo_2(DAniF)_2]_2(\mu$-X)$_4$, X = Cl (**1**), Br (**2**), and I (**3**). All three compounds show two reversible one-electron oxidation processes with potential separations ($\Delta E_{1/2}$) between the two oxidation processes of 540, 499, and 440 mV, respectively. These $\Delta E_{1/2}$ values show that the strength of the electronic coupling between the dimetal units decreases as the $Mo_2\cdots Mo_2$ distance increases from **1** to **2**, and then to **3**. The structures, EPR spectra, and near-IR (NIR) spectra of the corresponding mixed-valence species (**1-PF$_6$**, **2-PF$_6$**, and **3-PF$_6$**) indicate that the clusters are electronically delocalized. Calculations at the DFT level indicate that the strong electronic communication is principally due to a direct overlap between the δ orbitals from the adjacent dimetal units.

Introduction

For some years there has been interest in understanding the effects of various variables in the electronic communication between two dimetal units joined by a linker such as a dicarboxylate, a dioxamidate, or other anions such as an anion MO_4^{2-}, M = S, Mo, W.[1] Such studies, as well as those of compounds having two single metal redox sites connected by one or more linkers, are of significance in a range of interdisciplinary areas for reasons that vary from augmenting fundamental knowledge of chemistry to the search for a better understanding of important biochemical redox and electron-transfer processes[2] to fabrication of nanoscale structures in materials science.[3]

The earliest studies were done on species such as the Creutz−Taube ion, a pyrazine-bridged diruthenium complex that was synthesized in the late 1960s;[4] a host of other such systems have since been investigated.[5] It is generally understood[6,7] that electronic interaction between two adjacent metal centers depends on geometric and bonding factors such as electrostatic interactions and electronic delocalization through the linker.[5,8]

The most frequently used dimetal unit, $[Mo_2(DAniF)_3]^+$,[9] contains a quadruply bonded dimolybdenum core (Mo_2^{4+})

* To whom correspondence should be addressed. E-mail: cotton@tamu.edu (F.A.C.); cyliu05@gmail.com (C.Y.L.); murillo@tamu.edu (C.A.M.).
† Texas A&M University.
‡ Tongji University.

(1) (a) Cotton, F. A.; Lin, C.; Murillo, C. A. *Acc. Chem. Res*. **2001**, *34*, 759. (b) Cotton, F. A.; Lin, C.; Murillo, C. A. *Proc. Natl. Acad. Sci. U.S.A.* **2002**, *99*, 4810. (c) Chisholm, M. H.; Macintosh, A. M. *Chem Rev.* **2005**, *105*, 2949.
(2) See for example: (a) Prassides, K., Ed. *Mixed-valency Systems. Applications in Chemistry, Physics and Biology*; Kluwer Academic Publishers: Dordrecht, The Netherlands, 1991. (b) Blondin, G.; Gired, J.-J. *Chem. Rev.* 1990, *90*, 1359 and references therein. (c) Gamelin, D. R.; Bominaar, E. L.; Kirk, M. L.; Wieghardt, K.; Solomon, E. I. *J. Am. Chem. Soc.* **1996**, *118*, 8085 and references therein.
(3) (a) Ward, M. D. *Chem. Soc. Rev.* **1995**, *34*, 121. (b) Astruc, D. *Acc. Chem. Res.* **1997**, *30*, 383. (c) McCleverty, J. A.; Ward, M. D. *Acc. Chem. Res.* **1998**, *31*, 842.
(4) (a) Creutz, C.; Taube, H. *J. Am. Chem. Soc.* **1969**, *91*, 3988. (b) Creutz, C.; Taube, H. *J. Am. Chem. Soc.* **1973**, *95*, 1086.
(5) See for example: (a) Creutz, C. *Prog. Inorg. Chem.* **1983**, *30*, 1. (b) Richardson, D. E.; Taube, H. *Coord. Chem. Rev.* **1984**, *60*, 107. (c) Dogan, A.; Sarkar, B.; Klein, A.; Lissner, F.; Schleid, T.; Fiedler, J.; Zalis, S.; Jain, V. K.; Kaim, W. *Inorg. Chem.* **2004**, *43*, 5973. (d) Chisholm, M. H.; Feil, F.; Hadad, C. M.; Patmore, N. J. *J. Am. Chem. Soc.* **2005**, *127*, 18150. (e) Rigaut, S.; Olivier, C.; Costuas, K.; Choua, S.; Fadhel, O.; Massue, J.; Turek, P.; Saillard, J.-Y.; Dixneuf, P. H.; Touchard, D. *J. Am. Chem. Soc.* **2006**, *128*, 5859. (f) D'Alessandro, D. M.; Dinolfo, P. H.; Davies, M. S.; Hupp, J. T.; Keene, F. R. *Inorg. Chem.* **2006**, *45*, 3261.
(6) (a) Crutchley, R. J. *Adv. Inorg. Chem.* **1994**, *41*, 273. (b) Kaim, W.; Klein, A.; Glöckle, M. *Acc. Chem. Res.* **2000**, *33*, 755. (c) Demadis, K. D.; Harshorn, M.; Meyer, T. *J. Chem. Rev.* **2001**, *101*, 2655.
(7) (a) Creager, S.; Yu, C. J.; Bamdad, C.; O'Connor, S.; MacLean, T.; Lam, E.; Chong, Y.; Olsen, G. T.; Luo, J.; Gozin, M.; Kayyem, J. F. *J. Am. Chem. Soc.* **1999**, *121*, 1059. (b) Launary, J.-P. *Chem. Soc. Rev.* **2001**, *30*, 386.
(8) Cotton, F. A.; Donahue, J. P.; Murillo, C. A.; Pérez, L. M. *J. Am. Chem. Soc.* **2003**, *125*, 5486.

10.1021/ic061304a CCC: $33.50
Published on Web 09/26/2006

Scheme 1

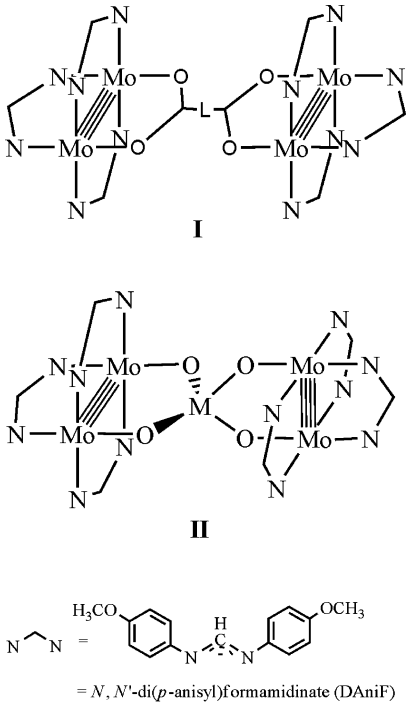

supported by three nonlabile *N*,*N*′-di-*p*-anisylformamidinate groups (DAniF), and it forms compounds of the type $[Mo_2(DAniF)_3]L[Mo_2(DAniF)_3]$ when L is an appropriate tetradentate group (Scheme 1). These compounds usually exhibit two successive one-electron oxidation processes corresponding to oxidation of one and then the other $[Mo_2]$ unit from a Mo_2^{4+} to a Mo_2^{5+} core.[10] The singly oxidized mixed-valence compounds formally resemble the Creutz−Taube ion in that they have "two charge-bearing units connected by a bridge".[11] For such compounds, the separation between electrode potentials ($\Delta E_{1/2}$) has been a common and useful guide to their classification as class I (localized) or class III (delocalized), or something in between (class II).

The situation is more complex and less understood for systems which have more than one linker, e.g., compounds such as $[cis\text{-}Mo_2(DAniF)_2]_2(\mu\text{-}Cl)_4$ (**1**).[12] For the singly oxidized complex $\{[cis\text{-}Mo_2(DAniF)_2]_2(\mu\text{-}Cl)_4\}PF_6$ (**1-PF$_6$**), already published in a communication,[13] it was found that upon oxidation of the neutral precursor the separation between the two dimetal units decreased by 0.23 Å. This is contrary to the expectation that an increase in charge would lead to an increase in Coulombic repulsion and a longer $[Mo_2]\cdots[Mo_2]$ separation, $[Mo_2] = cis\text{-}Mo_2(DAniF)_2$. More recently, we observed similar decreases in $[Mo_2]\cdots[Mo_2]$ separations occurring upon oxidation of $[cis\text{-}Mo_2(DAniF)_2]_2(\mu\text{-}OMe)_4$[14] and $[Mo_2(DAniF)_3]_2(\mu\text{-}H)_2$.[15] For these compounds, DFT calculations suggested partial bond formation, directly between the Mo_2 units, as oxidation takes place.

Here we report further studies on **1** and **1-PF$_6$** and the syntheses of the Br analogues $[cis\text{-}Mo_2(DAniF)_2]_2(\mu\text{-}Br)_4$ (**2**) and its oxidized product **2-PF$_6$**. We complete the series by oxidizing $[cis\text{-}Mo_2(DAniF)_2]_2(\mu\text{-}I)_4$ (**3**) to **3-PF$_6$**. Structures are provided for the new compounds. Electrochemical data for all isostructural neutral compounds and NIR data for the three mixed-valence species are also presented. DFT calculations support partial formation of long-range Mo-to-Mo bonds as oxidation occurs. For comparison, DFT calculations are also provided for $[Mo_2Cl_2(PEt_3)_2]_2(\mu\text{-}Cl)_4$,[16] which is known to have a rectangular arrangement of molybdenum atoms with triple and single Mo_2 bonds alternating around the rectangle. The series of compounds $[cis\text{-}Mo_2(DAniF)_2]_2(\mu\text{-}X)_4$, X = Cl, Br, and I, which are the subject of this work, provide a rare opportunity for evaluation of electronic communication in a very similar environment where the size of the halide bridging ligands allows us to tune the direct orbital overlap interaction between dimetal units.

Results and Discussion

Syntheses. Compounds **1**, **2**, and **3** were previously prepared by cumbersome synthetic methods that involved either reduction of $Mo_2(DAniF)_3Cl_2$ with KC_8 in the presence of $ClSiMe_3$ or reaction of $Mo_2(DAniF)_4$ with $XSiMe_3$ (X = Br, I) over a period of 2 days.[12] The use of the reaction described by eq 1, which follows a procedure reported in a

$$2[cis\text{-}Mo_2(DAniF)_2(CH_3CN)_4](BF_4)_2 + 4Bu^n{}_4NX\ (X = Cl, Br, \text{and } I) \rightarrow [cis\text{-}Mo_2(DAniF)_2]_2(\mu\text{-}X)_4 + 4Bu^n{}_4NBF_4 + 8CH_3CN \quad (1)$$

communication for **1**, is far more convenient.[13] This procedure, based on the use of the designed dimolybdenum building block $[cis\text{-}Mo_2(DAniF)_2(CH_3CN)_4]^{2+}$,[17] is general and straightforward for the syntheses of all three compounds, as the halides simply displace labile acetonitrile molecules from the dimetal unit and bring the two $[Mo_2]$ units together. However, it is important to use very dry starting materials and solvents to obtain pure products. Because the neutral products have low solubility in polar solvents, e.g., ethanol and acetonitrile, there is an additional driving force for the reaction to proceed.

(9) (a) Cotton, F. A.; Donahue, J. P.; Lin, C.; Murillo, C. A. *Inorg. Chem.* **2001**, *40*, 1234. (b) Cotton, F. A.; Donahue, J. P.; Murillo, C. A. *J. Am. Chem. Soc.* **2003**, *125*, 5436. (c) Cotton, F. A.; Donahue, J. P.; Murillo, C. A. *Inorg. Chem.* **2001**, *40*, 2229. (d) Cotton, F. A.; Liu, C. Y.; Murillo, C. A.; Wang, X. *Inorg. Chem.* **2003**, *42*, 4619. (e) Cotton, F. A.; Daniels, L. M.; Donahue, J. P.; Liu, C. Y.; Murillo, C. A. *Inorg. Chem.* **2002**, *41*, 1354.

(10) (a) Cotton, F. A.; Murillo, C. A.; Walton, R. A. *Multiple Bonds between Metal Atoms*, 3rd ed.; Springer Science and Business Media, Inc.: New York, 2005. (b) Cotton, F. A.; Liu, C. Y.; Murillo, C. A.; Villagrán, D.; Wang, X. *J. Am. Chem. Soc.* **2004**, *126*, 14822.

(11) Nelsen, S. F. *Chem. Eur. J.* **2000**, *4*, 581.

(12) Cotton, F. A.; Daniels, L. M.; Guimet, I.; Henning, R. W.; Jordan, IV, G. T.; Lin, C.; Murillo, C. A.; Schultz, A. J. *J. Am. Chem. Soc.* **1998**, *120*, 12531.

(13) Cotton, F. A.; Liu, C. Y.; Murillo, C. A.; Wang, X. *Chem. Commun.* **2003**, 2190.

(14) Cotton, F. A.; Li, Z.; Liu, C. Y.; Murillo, C. A.; Zhao, Q. *Inorg. Chem.* **2006**, *45*, 6387.

(15) Cotton, F. A.; Donahue, J. P.; Huang, P.; Murillo, C. A.; Villagrán, D. *Z. Anorg. Allg. Chem.* **2005**, *631*, 2606.

(16) (a) McGinnis, R. N.; Ryan, T. R.; McCarley, R. E. *J. Am. Chem. Soc.* **1978**, *100*, 7900. (b) Cotton, F. A.; Shang, M. *J. Cluster Sci.* **1991**, *2*, 121.

(17) Chisholm, M. H.; Cotton, F. A.; Daniels, L. M.; Folting, K.; Huffman, J. C.; Iyer, S. S.; Lin, C.; Macintosh, A. M.; Murillo, C. A. *J. Chem. Soc., Dalton Trans.* **1999**, 1387.

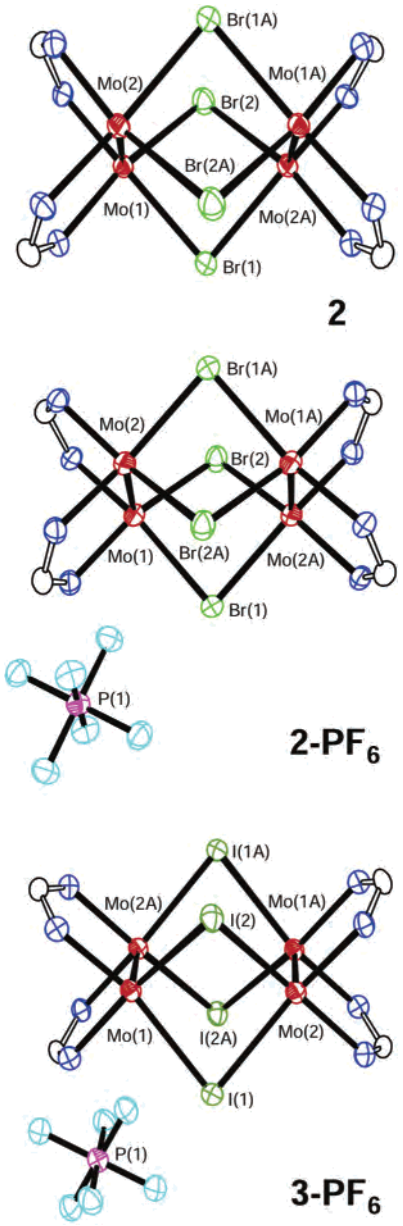

Figure 1. Core structures of **2**·$2CH_2Cl_2$, **2-PF$_6$**·$2CH_2Cl_2$, and **3-PF$_6$**·$2CH_2Cl_2$ drawn with ellipsoids at the 40% probability level. All *p*-anisyl groups and hydrogen atoms have been omitted for clarity.

Oxidation of the neutral compounds having X = Br and I with 1 equiv of $FcPF_6$ produces the singly oxidized species $\{[cis\text{-}Mo_2(DAniF)_2]_2(\mu\text{-}X)_4\}PF_6$, X = Br (**2-PF$_6$**) and I (**3-PF$_6$**).

Structural Results. Compound **2** crystallizes in the monoclinic space group $P2_1/n$ with $Z = 2$, which requires the molecule to have a crystallographic inversion center. The core of the structure, shown in Figure 1, consists of two $[Mo_2]$ units linked by four Br atoms. The core has idealized D_{2h} symmetry and is similar to those in **1** and **3**.[12] The crystallographically equivalent Mo−Mo quadruple bond distances, 2.1181(6) Å, are also similar to those of **1** and **3** but about 0.02 Å longer than those in dimolybdenum paddlewheel compounds supported by four three-atom bridging ligands, such as $Mo_2(O_2CCH_3)_4$[18] and $Mo_2(DAniF)_4$.[19] The nonbonding separations between the midpoints of the quadruple bonds for the three compounds are 3.601, 3.697, and 3.915 Å for **1**, **2**, and **3**, respectively, and they increase as the atomic radius of the bridging atom increases from Cl to I via Br (Table 1). These separations are significantly shorter than those in molybdenum-containing pairs (also known as "dimers of dimers") in group **I**- and **II**-type compounds (Scheme 1). Among these, the shortest separation is found for L = oxalate (6.94 Å).[9a] The Mo−X distances are 2.516[2], 2.649[2], and 2.845[2] Å for **1**, **2**, and **3**, respectively. The average X−Mo−X angles increase slightly from 81.06[3]° to 82.95[2]° to 83.89[2]° from the Cl to the Br to the I analogue, while the average Mo−X−Mo angles decrease from 91.42[5]° to 88.50[2]° to 87.02[2]° in the same order. These angles are consistent with the increase of atomic radii from Cl to Br, then to I.

The ^{1}H NMR spectra show singlets for both the methine protons (ca. 8.6 ppm) and methoxyl groups (ca. 3.7 ppm). This suggests that the D_{2h} symmetry of the $[Mo_2](\mu\text{-}X)_4[Mo_2]$ molecules persists in solution, as all ligand anisyl groups are equivalent.

The mixed-valence complex **2-PF$_6$** crystallizes in triclinic space group $P\bar{1}$ (Figure 1). The cation and anion reside on different inversion centers. Upon removal of one electron, the two Mo−Mo bond distances are lengthened from 2.1181(6) Å in the precursor to 2.1406(9) Å. This lengthening is consistent with an electron being removed from the δ orbitals of the dimetal units and a decrease of 0.25 in overall bond order. The increase of 0.023 Å in the Mo−Mo bond distance in going from **2** to **2-PF$_6$** is similar to those observed in delocalized systems but considerably less than those found in localized mixed-valence complexes of the type $[Mo_2]^+L\text{-}[Mo_2]^0$.[9,20] The metal−ligand bond distances also appear to be shortened, for example, from 2.649[2] to 2.622[2] Å for Mo−Br and from 2.093[5] to 2.091[4] Å for Mo−N_{DAniF} because of the increase of the oxidation state of the dimetal units, but these changes are very small. Accompanying the increase of the metal−metal bond distance, the separation between the midpoints of the two $[Mo_2]$ units ($Mo_2\cdots Mo_2$) is reduced by about 0.21 Å, from 3.697 to 3.488 Å. The average bridging angles Mo−Br−Mo (83.38[2]°) are smaller than those in the precursor (88.50[2]°). Similar changes on the geometry have been observed for the iodine analogue as one electron is removed from the neutral complex.

Magnetism and NIR Spectra. The X-band EPR spectra for **2-PF$_6$** and **3-PF$_6$** were measured at room temperature in CH_2Cl_2 solution. Only one prominent signal was observed for each complex, which is consistent with a doublet electronic ground state. The *g* values of 1.935 for **2-PF$_6$** and 1.959 for **3-PF$_6$** are significantly different from that for an organic free radical and indicate that the unpaired electron resides in a mainly metal-based orbital. The main peak is due to molecules containing only the ^{96}Mo ($I = 0$) isotope

(18) Cotton, F. A.; Mester, Z. C.; Webb, T. R. *Acta Crystallogr.* **1974**, *B30*, 2768.
(19) Lin, C.; Protasiewicz, J. D.; Smith, E. T.; Ren, T. *Inorg. Chem.* **1996**, *35*, 6422.
(20) (a) Cotton F. A.; Li, Z.; Liu, C. Y.; Murillo, C. A.; Villagrán, D. *Inorg. Chem.* **2006**, *45*, 767. (b) Cotton, F. A.; Murillo, C. A.; Villagrán, D.; Yu, R. *J. Am. Chem. Soc.* **2006**, *128*, 3281.

Table 1. Selected Bond Distances (Å) and Angles (deg)

compound	Mo−Mo	$Mo_2\cdots Mo_2$[a]	Mo−X[b]	Mo−N	Mo−X−Mo	ref
1	2.1191(4)	3.601	2.516[2]	2.095[5]	91.42[5]	13
1-PF$_6$	2.1453(3)	3.374	2.490[6]	2.083[3]	85.28[1]	13
2	2.1181(6)	3.697	2.649[2]	2.093[5]	88.50[2]	this work
2-PF$_6$	2.1406(9)	3.488	2.622[2]	2.091[4]	83.38[2]	this work
3	2.117(1)	3.915	2.845[2]	2.100[6]	87.02[2]	12
3-PF$_6$	2.144(1)	3.632	2.812[2]	2.104[8]	80.50[4]	this work
$[Mo_2Cl_2(PEt_3)_2]_2(\mu\text{-}Cl)_4$	2.211(3)	2.901	2.401[6]		74.50	16

[a] Distance between midpoints of the dimolybdenum bonds. [b] X = bridging anion.

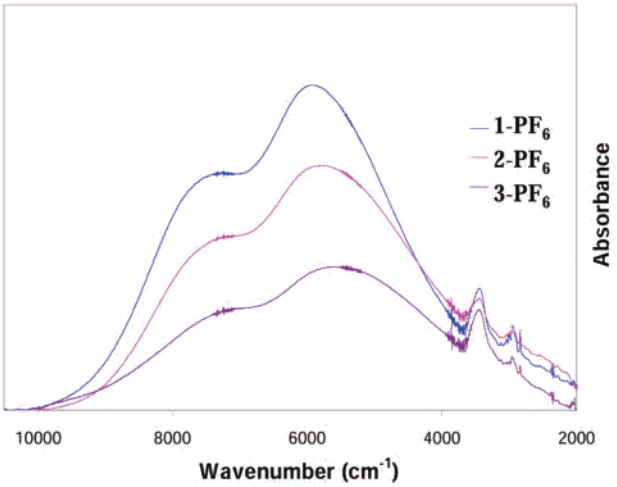

Figure 2. Near-IR spectra of the crystalline mixed-valence species **1-PF$_6$**, **2-PF$_6$**, and **3-PF$_6$** in KBr pellets.

(about 74% abundance), whereas the small peaks flanking the main signal are due to coupling of four Mo (^{95,97}Mo (I = 5/2) isotopes that have combined natural abundance of about 25%) and four halide atoms. This is again consistent with the electron being delocalized over the two [Mo_2] units.

The NIR spectra of **1-PF$_6$**, **2-PF$_6$**, and **3-PF$_6$** were measured in the region from 2000 to 10500 cm^{-1} both in the solid state using KBr pellets (Figure 2 and Table S1) and in CH_2Cl_2 solutions. In both media, the NIR spectra were essentially the same. Each mixed-valence complex shows two intense broad absorption bands centered at ca. 5700 and 7200 cm^{-1}. It is similar to the NIR spectra of the complex $\{[cis\text{-}Mo_2(DAniF)_2]_2(\mu\text{-}OMe)_4\}^+$ where two broad absorption bands were observed in the NIR region.[14] Such transitions are often referred to as intervalence charge-transfer transitions. The spectra of these three mixed-valence species are qualitatively different from those for the [Mo_2]L[Mo_2] systems, for which only one band has been observed in the NIR region.[20,21] Even though the Hush formula, $\Delta\nu_{1/2} = (2310\nu_{max})^{1/2}$,[22] may not be used to interpret the spectra of these $[cis\text{-}Mo_2(DAniF)_2]_2(\mu\text{-}X)_4$ compounds, the intense bands are consistent with significant electronic interaction between the two dimolybdenum units.

Electrochemistry. The CVs of **2** and **3** are shown in Figure 3, and the electrochemical data for the three compounds are listed in Table 2. These compounds exhibit two

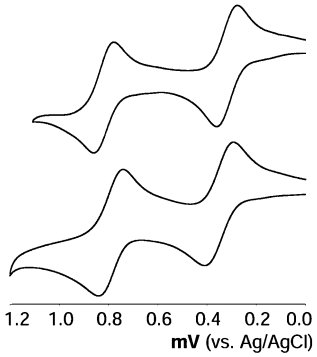

Figure 3. Cyclic voltammogram for **2** (upper) and **3** (lower) in CH_2Cl_2 solution.

Table 2. Oxidation Potentials and Comproportionation Constants for **1**, **2**, and **3** along with Separations between Dimetal Units

	$Mo_2\cdots Mo_2$ (Å)	$E_{1/2}(1)$ (mV)	$E_{1/2}(2)$ (mV)	$\Delta E_{1/2}$ (mV)	K_C	ref
1	3.601	260	800	540	1.3×10^9	13
2	3.697	314	813	499	2.7×10^8	this work
3	3.915	350	790	440	2.7×10^7	this work

well-separated redox couples, corresponding to two one-electron oxidation processes occurring on the two [Mo_2] units. For **1**, **2**, and **3**, the potential separations ($\Delta E_{1/2}$) between the two oxidation processes are 540, 499, and 440 mV, respectively. These very large $\Delta E_{1/2}$ values suggest that there is strong electronic coupling between the two [Mo_2] units. From the values of $\Delta E_{1/2}$, comproportionation constants (K_C) for the equilibrium in eq 2 can be derived.[23] Their magnitudes, ranging from 10^9 to 10^7, are listed in Table 2. Clearly, these singly oxidized species are thermodynamically highly stable, and it is reasonable to make the assumption that the stability is due to delocalization of the charge.

$$\{[Mo_2]_2(\mu\text{-}X_4)\}^{2+} + [Mo_2]_2(\mu\text{-}X_4) \rightleftharpoons 2\{[Mo_2]_2(\mu\text{-}X_4)\}^{+} \quad (2)$$

$$K_C = e^{\Delta E_{1/2}/25.69}$$

It has been established in many other cases that back-bonding from the metal centers to the linker, e.g., $\delta \rightarrow \pi^*$ for systems with dimetal units[8,10] and d_{xz}, $d_{yz} \rightarrow \pi^*$ for linked mononuclear compounds,[5] is the major pathway by which electronic communication between the two metal centers occurs. Similar back-bonding is not expected for the $[Mo_2]_2(\mu\text{-}X_4)$ species because of the nature of the linkers, nor is the geometric relationship of the dimolybdenum building

(21) Chisholm, M. H.; Pate, B. D.; Wilson, P. J.; Zalesky, J. M. *Chem. Commun.* **2002**, 1084.
(22) The Hush formula is appropriate for systems with two dimetal units linked by *one* linker. See: Hush, N. S. *Coord. Chem. Rev.* **1985**, *64*, 135.
(23) Richardson, D. E.; Taube, H. *Inorg. Chem.* **1981**, *20*, 1278.

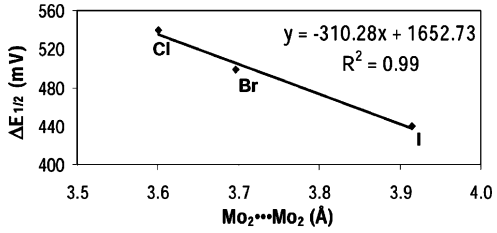

Figure 4. $\Delta E_{1/2}$ values versus the distances between the midpoints of the $[Mo_2]$ units, $Mo_2\cdots Mo_2$, in $[cis\text{-}Mo_2(DAniF)_2]_2X_4$ (X = Cl, Br, and I).

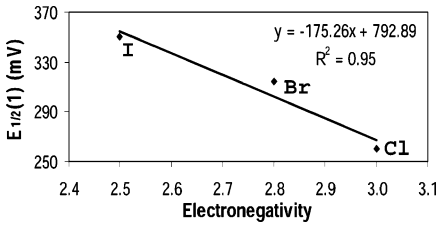

Figure 5. $E_{1/2}(1)$ values (mV) as a function of electronegativity of the μ-X atoms: Cl, Br, and I.

blocks to each other conducive to strong coupling via the linkers. Therefore, the explanation for the strong electronic coupling observed in these species must be different.

It appears that the short metal-to-metal separations promote strong electrostatic interactions; hence, it is one of the major factors that enhance the electronic coupling over the two $[Mo_2]$ units. It is noted also that some lobes of the δ orbitals from the two $[Mo_2]$ units are pointing directly toward each other, as shown in Scheme 2. Given the short $Mo_2\cdots Mo_2$ distances (3.6−3.9 Å) and the D_{2h} molecular symmetry, it appears that electron delocalization may occur via a direct metal-to-metal σ interaction. Electron delocalization in this complex system is supported by the X-ray structural analysis of the mixed-valence species **1-PF$_6$**,[13] **2-PF$_6$**, and **3-PF$_6$**.

For this series of compounds, the coupling effect decreases as the atomic number of the bridging atom X increases. Figure 4 shows that the $\Delta E_{1/2}$ values are nearly linearly related to the distances between $[Mo_2]$ units (d in Å), and the $\Delta E_{1/2}$ values decrease as d increases with an increase in the atomic radius of X. The trend in the $\Delta E_{1/2}$ values appears reasonable regardless of whether an electrostatic interaction or a direct metal-to-metal σ interaction between two $[Mo_2]$ units or both are responsible for the electronic coupling. Also, the bridging atom (X) has an influence on the first redox process, $E_{1/2}^{(+1/0)}$, and these $E_{1/2}(1)$ values are nearly a linear function of the electronegativity of the halogen atom, as shown in Figure 5.

Electronic Structures and DFT Calculations. A series of DFT calculations and fragment analysis was carried out

Scheme 2

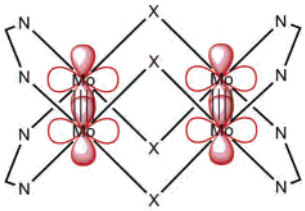

III

to better understand the electronic interaction between the $[Mo_2]$ units. Geometry optimizations for the neutral and singly oxidized species were done using the parameters from the crystal structures as starting points. The models, with all anisyl groups replaced by hydrogen atoms, were simplified to $[cis\text{-}Mo_2(NHCHNH)_2]_2(\mu\text{-}X)_4$ (X = Cl, Br, I) having D_{2h} symmetry.

The general agreement between the calculated and the experimental geometric data shown in Tables 1 and 3 suggests that such a simplification is reasonable. The overestimation of the Mo−Mo distances (ca. 0.04 Å) is reasonable because of the use of hydrogen atoms in the theoretical study instead of the basic *p*-anisyl groups. All changes in bond distances and angles resulting from the oxidation are in good agreement with those from X-ray crystallography. After one electron was removed in the halide-bridged complexes, the calculated distances between the midpoints of the two $[Mo_2]$ units decreased by about 0.21−0.27 Å; these changes are comparable with the experimental decreases which are ca. 0.21−0.28 Å.

Analysis of the frontier orbitals from the calculations (Figures 6 and 7) indicates that direct σ interaction through space occurs between the δ orbitals in the dimetal units. The two filled δ orbitals interact with each other and generate two molecular orbitals, one bonding (a_g, $\delta + \delta$) and one antibonding (b_{3u}, $\delta - \delta$) over the four molybdenum atoms. The combination of the two δ^* orbitals gives two more molecular orbitals, which again include one bonding (b_{2u}, $\delta^* + \delta^*$) and one antibonding (b_{1g}, $\delta^* - \delta^*$). The orbitals from the molybdenum atoms make the largest contribution to these two sets of MOs (ca. 70−87%). The frontier orbitals for $[cis\text{-}Mo_2(NHCHNH)_2]_2(\mu\text{-}Cl)_4$ are shown in Figure 7a, in which the in-phase combination of the δ orbitals (a_g, $\delta + \delta$), is the HOMO-1, whereas the HOMO is the out-of-phase combination of the δ orbitals (b_{3u}, $\delta - \delta$). There would be no bonding between the two $[Mo_2]$ units, with each dimolybdenum unit remaining quadruply bonded. The energy difference, ΔE, between $\delta - \delta$ and $\delta + \delta$ orbitals, is a measure of the electronic interaction between the two dimetal

Table 3. Calculated Bond Lengths (Å) and Angles (deg) for Models of **1**, **2**, **3** and $[Mo_2Cl_2(PMe_3)_2]_2(\mu\text{-}Cl)_4$

	charge	Mo−Mo	$Mo_2\cdots Mo_2$	Mo−X[a]	Mo−X−Mo
1	0	2.160	3.706	2.594	91.17
	+1	2.181	3.503	2.556	86.52
2	0	2.161	3.864	2.765	88.66
	+1	2.182	3.632	2.721	83.72
3	0	2.163	4.054	2.975	85.89
	+1	2.184	3.780	2.921	80.63
$[Mo_2Cl_2(PMe_3)_2]_2(\mu\text{-}Cl)_4$	0	2.240	2.918	2.453	72.98

[a] X = bridging anion.

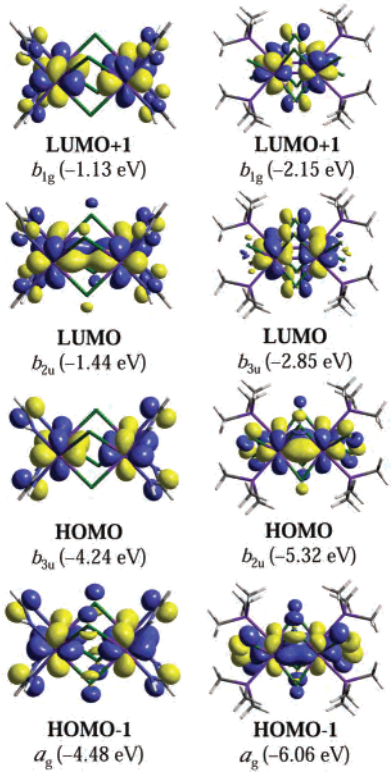

Figure 6. Selected frontier orbitals for the models [*cis*-$Mo_2(NHCHNH)_2]_2Cl_4$ (left) and $[Mo_2Cl_2(PMe_3)_2]_2(\mu\text{-}Cl)_4$ (right) using an isosurface value of 0.03.

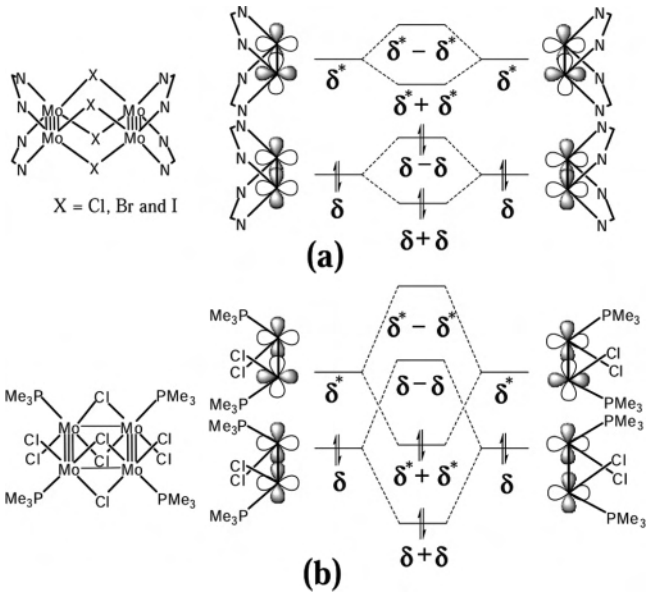

Figure 7. Orbital interaction diagram for [*cis*-$Mo_2(NHCHNH)_2]_2X_4$ (X = Cl, Br, I) (upper) and $[Mo_2Cl_2(PMe_3)_2]_2(\mu\text{-}Cl)_4$ (lower). The two dimetal units are shown in the left and right columns, respectively.

units.[15,20] The calculations (Table 4) show that the ΔE values are 0.21, 0.23, and 0.25 eV for **3**, **2**, and **1**, respectively. This indicates that the electronic coupling between the two dimetal units increases as the two dimetal units approach each other, as would be expected from the shortening of the $Mo_2\cdots Mo_2$ distances.

To obtain the detailed relationship between the ΔE values and the $Mo_2\cdots Mo_2$ distance, a fragment analysis and comparative study were carried out. The calculations were done at the DFT level using a model that brought together two $[Mo_2(HNCHNH)_2]^{2+}$ components devoid of linking atoms but having the same relative orientation than that in $[Mo_2(NHCHNH)_2]_2(\mu\text{-}Cl)_4$. When the $Mo_2\cdots Mo_2$ distance was varied, the ΔE values changed. The calculation indicates that when the $Mo_2\cdots Mo_2$ distance is equal to or larger than 9 Å (green region in Figure 8), there is no direct interaction between the two dimetal units; the two δ orbitals have the same energy, and the ΔE values are essentially zero. When the two $[Mo_2]$ units approach each other (red region), the direct σ interaction affects the energy of the two δ orbitals. The two δ orbitals form a set of molecular orbitals $\delta + \delta$ and $\delta - \delta$, where the two δ^* orbitals form $\delta^* + \delta^*$ and $\delta^* - \delta^*$ MOs. The ΔE (y axis, $E_{\delta-\delta} - E_{\delta+\delta}$) values slowly increase at first and then rise quickly until the $Mo_2\cdots Mo_2$ distance (x axis) reaches 3.12 Å. In that state, there is direct σ interaction between the two $[Mo_2]$ units and the strength of the interaction increases even more rapidly as the $Mo_2\cdots Mo_2$ distance decreases. As the two dimetal units approach each other, the energy difference between the orbitals of $\delta - \delta$ and $\delta^* + \delta^*$ will be smaller because of the increase in the ΔE values. At some point, the order of these two orbitals will be switched. The calculations show that when the $Mo_2\cdots Mo_2$ distance is less than 3.12 Å (blue region), the $\delta^* + \delta^*$ orbital becomes the HOMO and $\delta - \delta$ is the LUMO. There is no longer a δ bond in each $[Mo_2]$ unit because there is equal electron density in the δ and δ^* orbitals. Simultaneously, two σ single bonds form between the two $[Mo_2]$ units, resulting in a rectangle with two single bonds and two triple bonds. This route resembles the 2 + 2 cycloaddition in the process of dimerization of ethylene to cyclobutane in which breaking of two pπ orbitals takes place and two new σ single bonds are formed.[24]

One example of this type of rectangle is $[Mo_2Cl_2(PEt_3)_2]_2(\mu\text{-}Cl)_4$[16] in which the short Mo−Mo bonds, not supported by bridging ligands, are 2.211(3) Å and the long bonds each bridged by two Cl atoms are 2.901(2) Å. Note that this distance is less than the calculated crossover state (3.12 Å). DFT calculations were performed on this molecule using the simplified model $[Mo_2Cl_2(PMe_3)_2]_2(\mu\text{-}Cl)_4$. The frontier orbitals analysis (Figure 7b) shows that the HOMO is indeed the in-phase combination of the δ^* orbitals (b_{2u}, $\delta^* + \delta^*$), whereas the LUMO is the antibonding combination of the δ orbitals (b_{3u}, $\delta - \delta$), and this complex is a tetrametal analogue of cyclobutadiyne as initially proposed.[16] The frontier MOs also show that none of the single bonds or the triple bonds can be viewed as isolated and that the four electrons on the HOMO and HOMO-1 are delocalized over the four molybdenum atoms.

For the singly oxidized cation $\{[cis\text{-}Mo_2(NHCHNH)_2]_2(\mu\text{-}Cl)_4\}^+$, the electronic structure (Figure S1) is similar to that of the precursor where the four metal-based frontier MOs are comprised mainly of the δ and δ^* orbitals from the two dimetal units. This is consistent with the EPR spectra of the mixed-valence complexes which show that the electron is

(24) Cotton, F. A. *Chemical* Applications of *Group Theory*, 3rd ed.; John Wiley and Sons: New York, 1990.

Table 4. Comparison of ΔE (eV) with Calculated Distances between [Mo_2] Units

	$Mo_2\cdots Mo_2$ (exptl)	$Mo_2\cdots Mo_2$ (calcd)	ΔE (eV)[a]	$\Delta E_{1/2}$ (mV)	ref
$Mo_4Cl_8(PMe_3)_4$	2.901(2)[16]	2.918	3.21	NA	this work
[*cis*-$Mo_2(DAniF)_2]_2(OCH_3)_4$	3.245	3.333	0.34	554	14
1	3.601	3.706	0.25	540	this work
2	3.697	3.864	0.23	499	this work
3	3.915	4.054	0.21	440	this work

[a] $\Delta E = E_{\delta-\delta} - E_{\delta+\delta}$.

in an orbital that has mainly metal character because of the low g values (1.912 for Cl,[13] 1.935 for Br, and 1.959 for I). Upon a one-electron oxidation of the neutral precursor, removal of the electron from this metal-based orbital results in the lengthening of bond distances within the multiply bonded Mo−Mo units. Simultaneously, because of the antibonding character ($\delta - \delta$) between the two adjacent [Mo_2] units, shortening of the $Mo_2\cdots Mo_2$ distances occurs between adjacent units.

The DFT calculations on the three singly oxidized species show that the spin density of the SOMO (Figures 9 and S2) is delocalized over the two dimolybdenum units in each case. Because the model used requires these two units to be equivalent, these results do not, in themselves, constitute evidence for delocalization.[25] They were not done with that objective in mind, but rather to support the belief that direct σ interaction provides an efficient route for the electronic communication between the redox centers.

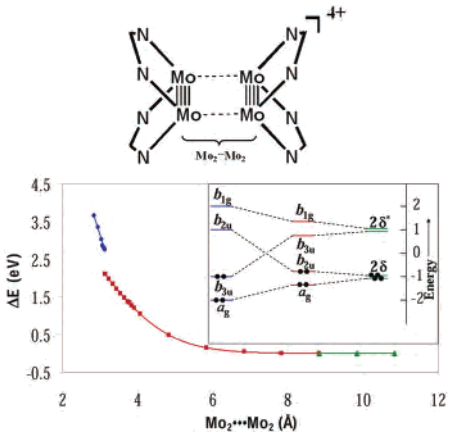

Figure 8. Comparison of the calculated ΔE ($E_{\delta-\delta} - E_{\delta+\delta}$) values versus the distance between the midpoints of the [Mo_2] units. In the inset, an orbital correlation diagram is given. Color code: green = two widely separated δ orbitals from two dimetal units; red = the two δ orbitals close enough for significant interactions to occur, blue = tetrametal analogue of cyclobutadiyne. The electron configurations correspond to the ground state for each state.

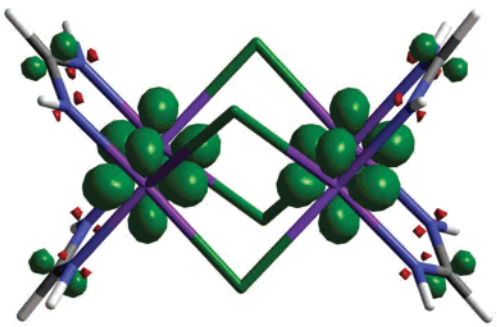

Figure 9. Spin density diagram of the SOMO in modes for **1-PF$_6$** with an isosurface value of 0.006.

Time-dependent (TD-DFT) calculations were also carried out on the halide-bridged complexes using the optimized geometry of the models [*cis*-$Mo_2(NHCHNH)_2]_2(\mu$-X)$_4$ (X = Cl, Br, I). Such calculations have been useful in understanding the electronic spectra of compounds having two [Mo_2] units linked by dicarboxylate groups.[8] As mentioned earlier, the three neutral species each show two weak absorption bands in the UV−vis range. The one observed at 495 nm for **1** is calculated at 552 nm for the two symmetry-allowed $\delta \rightarrow \delta^*$-type transitions that are close in energy, namely HOMO to LUMO+1 ($\delta - \delta \rightarrow \delta^* - \delta^*$) and HOMO-1 to LUMO ($\delta + \delta \rightarrow \delta^* + \delta^*$). The higher energy one, observed at ca. 390 nm and calculated at 452 nm, is a $\delta \rightarrow \pi^*$ transition (HOMO → LUMO+2).[26] For **2** and **3**, similar transitions were calculated.

For the mixed-valence species **1-PF$_6$**, the band at 600 nm is assigned to a LMCT band from the ligand-based orbital HOMO-4 → SOMO which is calculated at 628 nm, while the band at 434 nm corresponds to the SOMO → LUMO+1 ($\delta - \delta \rightarrow \delta^* - \delta^*$) transition. Similar transitions were calculated for **2-PF$_6$** and 3-**PF$_6$**. Two absorptions are predicted in the NIR range, and these bands appear experimentally in the electronic spectra at ca. 5700 and 7200 cm^{-1}, as shown in Figure 2. The more intense band centered at ca. 5700 cm^{-1} is the HOMO-1 → SOMO transition. The one centered at ca. 7200 cm^{-1} is tentatively assigned to HOMO-1 → LUMO ($\delta + \delta \rightarrow \delta^* + \delta^*$) on the basis of the calculated orbital energies and their symmetry given in Table S1. For these two transitions in {[*cis*-$Mo_2(NHCHNH)_2]_2(\mu$-X)$_4$}$^+$ cations, the calculations show that the energies (eV) decrease from 0.745 and 0.762 in **1**$^+$, to 0.717 and 0.753 in **2**$^+$, then to 0.651 and 0.748 in **3**$^+$, which follow the experimental trend.

Concluding Remarks. We have shown that, upon oxidation of the compounds [*cis*-$Mo_2(DAniF)_2]_2(\mu$-X)$_4$, X = Cl, Br, I, to species containing the corresponding {[*cis*-$Mo_2(DAniF)_2]_2(\mu$-X)$_4$}$^+$ cations, the separation between dimetal units ([Mo_2]$\cdots$[Mo_2]) decreases despite the increase in electrostatic charge. The decrease is caused by an increase in electronic communication which is principally due to a direct overlap between the δ orbitals from the adjacent dimetal units which leads to partial bond formation. In these compounds the $\Delta E_{1/2}$ values decrease as $Mo_2\cdots Mo_2$ increases with an increase in the atomic radius of X.

Experimental Section

Materials and Methods. Solvents were dried and then distilled under N_2 following conventional methods or purified under argon

(25) We thank a reviewer for emphasizing this point.
(26) LUMO+2 is the in-phase combination of the two π^* orbital from Mo_2 units.

Table 5. X-ray Crystallographic Data for **2**, **2-PF$_6$**, and **3-PF$_6$**

compound	**2**·2CH_2Cl_2	**2-PF$_6$**·2CH_2Cl_2	**3-PF$_6$**·2CH_2Cl_2
formula	$C_{62}H_{64}Br_4Cl_4Mo_4N_8O_8$	$C_{62}H_{64}Br_4Cl_4F_6Mo_4N_8O_8P$	$C_{62}H_{64}Cl_4F_6I_4Mo_4N_8O_8P$
fw	1894.41	2039.38	2227.34
space group	$P2_1/n$ (No. 14)	$P\bar{1}$ (No. 2)	$P\bar{1}$ (No. 2)
a (Å)	11.8343(19)	9.895(4)	9.247(2)
b (Å)	12.405(2)	12.165(4)	13.224(3)
c (Å)	23.934(4)	15.609(6)	15.417(3)
α (deg)	90	81.771(6)	89.677(4)
β (deg)	98.568(3)	85.841(6)	79.545(4)
γ (deg)	90	78.464(7)	81.104(4)
V (Å^3)	3474(1)	1820(1)	1831.1(7)
Z	2	1	1
T (K)	213	213	213
d_{calcd} (g/cm^3)	1.811	1.861	2.020
μ (mm^{-1})	3.217	3.110	2.595
R1[a] (wR2[b])	0.042 (0.106)	0.032 (0.089)	0.049 (0.108)

[a] $R1 = \sum||F_o| - |F_c||/\sum|F_o|$. [b] $wR2 = [\sum[w(F_o^2 - F_c^2)^2]/\sum[w(F_o^2)^2]]^{1/2}$.

using a Glass Contour solvent purification system. All synthetic operations were conducted under N_2 using Schlenk line techniques. [*cis*-Mo_2(DAniF)$_2$(NCCH_3)$_4$](BF_4)$_2$ was prepared by a published method;[17] **1** and **1-PF$_6$** were prepared as reported earlier,[13] the commercially available salts Bu$^n_4$NX (X = Cl, Br, I), were dried overnight at 50 °C under vacuum.

Physical Measurements. Elemental analyses were performed by Robertson Microlit Laboratories, Madison, NJ. ^{1}H NMR spectra were recorded on a Mercury-300 NMR spectrometer with chemical shifts (ppm) referenced to $CDCl_3$. Electronic spectra in CH_2Cl_2 were measured in the range of 200−800 nm on a Shimadzu UV-2501PC spectrophotometer. The NIR spectra were obtained from a Bruker TEASOR 27 spectrometer. Cyclic voltammograms (CVs) were collected on a CH Instruments electrochemical analyzer with Pt working and auxiliary electrodes, an Ag/AgCl reference electrode, a scan rate of 100 mV/s (for CVs), and 0.1 M Bu$_4$NPF_6 (in CH_2Cl_2) as electrolyte. Under these experimental conditions, the $E_{1/2}$ ferrocene/ferrocenium (Fc^+/Fc) couple was measured at 440 mV. EPR spectra were recorded using a Bruker ESP300 spectrometer.

Preparation of [*cis*-Mo$_2$(DAniF)$_2$]$_2$(μ-Br)$_4$, 2. To a mixture of 0.416 g (0.400 mmol) of [*cis*-Mo_2(DAniF)$_2$(CH_3CN)$_4$](BF_4)$_2$ and an excess of Bu$^n_4$NBr (0.644 g, 2.00 mmol) was added 20 mL of ethanol. A red-brown precipitate formed immediately upon stirring. The mixture was stirred at room temperature for 2 h. The supernatant solution was then decanted, and the brown solid was washed twice with 15 mL of ethanol and dried under vacuum. Large dark-red crystals were obtained by slow diffusion of hexanes into a CH_2Cl_2 solution of the product. Yield: 0.25 g (72%). ^{1}H NMR ($CDCl_3$, 300 MHz): 8.637 (s, 4H, −NC*H*N−), 6.683 (m, 16H, aromatic C-*H*), 6.603 (m, 16H, aromatic C-*H*), 3.678(s, 24H, −OCH_3); UV−vis, λ_{max} (nm) (ϵ, M^{-1} cm^{-1}): 394 (2.5 × 10^3), 500 (3.9 × 10^3). Anal. Calcd for $C_{60}H_{60}Br_4Mo_4N_8O_8$ (**2**): C, 41.79; H, 3.51; N, 6.50. Found: C, 41.87; H, 3.47; N, 6.33.

Preparation of [*cis*-Mo$_2$(DAniF)$_2$]$_2$(μ-I)$_4$, 3. This compound was prepared similarly to **2** using 0.416 g (0.400 mmol) of [*cis*-Mo_2(DAniF)$_2$(CH_3CN)$_4$](BF_4)$_2$ and an excess of Bu$^n_4$NI (0.738 g, 2.00 mmol) in 20 mL of ethanol. Yield: 0.36 g (94%). ^{1}H NMR ($CDCl_3$, 300 MHz): 8.555 (s, 4H, −NC*H*N−), 6.659 (m, 16H, aromatic C−*H*), 6.595 (m, 16H, aromatic C−*H*), 3.678(s, 24H, −OCH_3); UV−vis, λ_{max} (nm) (ϵ, M^{-1} cm^{-1}): 403 (3.4 × 10^3), 508 (3.8 × 10^3).

Preparation of {[*cis*-Mo$_2$(DAniF)$_2$]$_2$(μ-Br)$_4$}PF$_6$, 2-PF$_6$. Solutions of **2** (0.17 g, 0.10 mmol) in 10 mL of CH_2Cl_2 and ferrocenium hexafluorophosphate, ($FcPF_6$, 0.036 g, 0.11 mmol) in 15 mL of CH_2Cl_2 were prepared separately and cooled to −78 °C. Transfer of the cold $FcPF_6$ solution through a cannula into the red solution of **2** produced a dark-brown solution. The resultant solution was stirred at low temperature for 30 min, and precooled hexanes (50 mL) were then added to produce a dark-brown precipitate. After the solvent was decanted, the solid residue was washed with 20 mL of hexanes and then dried under vacuum. This solid was dissolved in 15 mL of dichloromethane at room temperature, and the solution was layered with 40 mL of hexanes. After about 1 week, block-shaped crystals were obtained. Yield: 0.16 g (85%). UV−vis, λ_{max} (nm) (ϵ, M^{-1} cm^{-1}): 478 (6.3 × 10^3), 619 (1.0 × 10^4). Anal. Calcd for $C_{61}H_{62}Br_4Cl_2F_6Mo_4N_8O_8P$ (**2-PF$_6$**·CH_2Cl_2): C, 37.49; H, 3.20; N, 5.73. Found: C, 37.75; H, 2.94; N, 5.57.

Preparation of {[*cis*-Mo$_2$(DAniF)$_2$]$_2$(μ-I)$_4$}PF$_6$, 3-PF$_6$. This black compound was synthesized using a procedure similar to that for **2-PF$_6$**. Small needle-shaped crystals of **3-PF$_6$**·2CH_2Cl_2 were obtained. Yield: 0.16 g (79%). UV−vis, λ_{max} (nm) (ϵ, M^{-1} cm^{-1}): 472 (5.2 × 10^3), 639 (9.3 × 10^3). Anal. Calcd for $C_{62}H_{64}I_4Cl_4F_6Mo_4N_8O_8P$ (**3-PF$_6$**·2CH_2Cl_2): C, 33.43; H, 2.90; N, 5.03. Found: C, 33.36; H, 2.56; N, 4.99.

X-ray Structure Determinations. Single crystals suitable for X-ray analysis were mounted and centered on the tips of cryoloops attached to a goniometer head. Data for **2**·2CH_2Cl_2, **2-PF$_6$**·2CH_2Cl_2, and **3-PF$_6$**·2CH_2Cl_2 were collected at −60 °C on a BRUKER SMART 1000 CCD area detector system. Cell parameters were determined using the program SMART.[27] Data reduction and integration were performed with the software package SAINT,[28] while absorption corrections were applied using the program SADABS.[29] The positions of the heavy atoms were found via direct methods using the program SHELXTL.[30] Subsequent cycles of least-squares refinement followed by difference Fourier syntheses revealed the positions of the remaining non-hydrogen atoms. Hydrogen atoms were added in idealized positions. Non-hydrogen atoms were refined with anisotropic displacement parameters. Crystallographic data for **2**·2CH_2Cl_2, **2-PF$_6$**·2CH_2Cl_2, and **3-PF$_6$**·2CH_2Cl_2 are given in Table 5 and selected bond distances and angles in Table 1.

(27) *SMART V 5.05 Software for the CCD Detector System*; Bruker Analytical X-ray System, Inc.: Madison, WI, 1998.
(28) *SAINT, Data Reduction Software, V 6.36A.*; Bruker Analytical X-ray System, Inc.: Madison, WI, 2002.
(29) *SADABS, Bruker/Siemens Area Detector Absorption and Other Corrections, V2.03*; Bruker Analytical X-ray System, Inc.: Madison, WI, 2002.
(30) Sheldrick, G. M. *SHELXTL. V 6.12*; Bruker Analytical X-ray Systems, Inc.: Madison, WI, 2000.

Computational Details. DFT[31] calculations were performed with the hybrid Becke's[32] three-parameter exchange functional and the Lee−Yang−Parr[33] nonlocal correlation functional (B3LYP) in the Gaussian 03 program.[34] Double-ζ-quality basis sets (D95)[35] were used on C, N, and H atoms as implemented in Gaussian. For P, Cl, and Br atoms, correlation-consistent double-ζ basis sets (CC-PVDZ)[36] were applied, where a double-ζ basis set (LANL2DZ) was applied on I atoms. A small effective core potential (ECP) representing the 1s2s2p3s3p3d core was used for the molybdenum atoms along with its corresponding double-ζ basis set (LANL2DZ).[37] TD-DFT calculations[38] were performed to assign the electronic spectra of these compounds. All calculations were performed on either Origin 3800 64-processor SGI or Origin 2000 32-processor SGI supercomputers located at the Texas A&M supercomputing facility.

Acknowledgment. We thank the Robert A. Welch Foundation and Texas A&M University for financial support. We also thank Dr. Dino Villagrán for his help with the theoretical calculations.

Supporting Information Available: X-ray crystallographic data for **2**·$2CH_2Cl_2$, **2-PF$_6$**·$2CH_2Cl_2$, and **3-PF$_6$**·$2CH_2Cl_2$ in standard CIF format. This material is available free of charge via the Internet at http://pubs.acs.org.

IC061304A

(31) (a) Hohenberg, P.; Kohn, W. *Phys. Rev.* **1964**, *136*, B864. (b) Parr, R. G.; Yang, W. *Density-Functional Theory of Atoms and Molecules*; Oxford University Press: Oxford, 1989.
(32) (a) Becke, A. D. *Phys. Rev. A* **1988**, *38*, 3098. (b) Becke, A. D. *J. Chem. Phys.* **1993**, *98*, 1372. (c) Becke, A. D. *J. Chem. Phys.* **1993**, *98*, 5648.
(33) Lee, C. T.; Yang, W. T.; Parr, R. G. *Phys. Rev. B* **1998**, *37*, 785.
(34) Frisch, M. J.; Trucks, G. W.; Schlegel, H. B.; Scuseria, G. E.; Robb, M. A.; Cheeseman, J. R.; Montgomery, J. A., Jr.; Vreven, T.; Kudin, K. N.; Burant, J. C.; Millam, J. M.; Iyengar, S. S.; Tomasi, J.; Barone, V.; Mennucci, B.; Cossi, M.; Scalmani, G.; Rega, N.; Petersson, G. A.; Nakatsuji, H.; Hada, M.; Ehara, M.; Toyota, K.; Fukuda, R.; Hasegawa, J.; Ishida, M.; Nakajima, T.; Honda, Y.; Kitao, O.; Nakai, H.; Klene, M.; Li, X.; Knox, J. E.; Hratchian, H. P.; Cross, J. B.; Bakken, V.; Adamo, C.; Jaramillo, J.; Gomperts, R.; Stratmann, R. E.; Yazyev, O.; Austin, A. J.; Cammi, R.; Pomelli, C.; Ochterski, J. W.; Ayala, P. Y.; Morokuma, K.; Voth, G. A.; Salvador, P.; Dannenberg, J. J.; Zakrzewski, V. G.; Dapprich, S.; Daniels, A. D.; Strain, M. C.; Farkas, O.; Malick, D. K.; Rabuck, A. D.; Raghavachari, K.; Foresman, J. B.; Ortiz, J. V.; Cui, Q.; Baboul, A. G.; Clifford, S.; Cioslowski, J.; Stefanov, B. B.; Liu, G.; Liashenko, A.; Piskorz, P.; Komaromi, I.; Martin, R. L.; Fox, D. J.; Keith, T.; Al-Laham, M. A.; Peng, C. Y.; Nanayakkara, A.; Challacombe, M.; Gill, P. M. W.; Johnson, B.; Chen, W.; Wong, M. W.; Gonzalez, C.; Pople, J. A. *Gaussian 03*, revision C.02; Gaussian, Inc.: Wallingford, CT, 2004.
(35) (a) Dunning, T. H.; Hay, P. J. In *Modern Theoretical Chemistry. 3. Methods of Electronic Structure Theory*; Schaefer, H. F., III, Ed.; Plenum Press: New York, 1977; pp 1−28. (b) Woon, D. E.; Dunning, T. H. *J. Chem. Phys.* **1993**, *98*, 1358.
(36) (a) Dunning, T. H. *J. Chem. Phys.* **1989**, *90*, 1007. (b) Woon, D. E.; Dunning, T. H. *J. Chem. Phys.* **1993**, *98*, 1358. (c) Wilson, A. K.; Woon, D. E.; Peterson, K. A.; Dunning, T. H. *J. Chem. Phys.* **1999**, *110*, 7667.
(37) (a) Wadt, W. R.; Hay, P. J. *J. Chem. Phys.* **1985**, *82*, 284. (b) Hay, P. J.; Wadt, W. R. *J. Chem. Phys.* **1985**, *82*, 299.
(38) Casida, M. E.; Jamorski, C.; Casida, K. C.; Salahub, D. R. *J. Chem. Phys.* **1998**, *108*, 4439.